PNAS RESEARCH ARTICLE | ENGINEERING OPEN ACCESS

Hydrophilic reentrant SLIPS enabled flow separation for rapid water harvesting

Zongqi Guo[a], Dylan Boylan[a], Li Shan[a], and Xianming Dai[a,1]

Edited by Steve Granick, Institute for Basic Science, Ulsan, South Korea; received June 4, 2022; accepted August 8, 2022

Water harvesting from air is desired for decentralized water supply wherever water is needed. When water vapor is condensed as droplets on a surface the unremoved droplets act as thermal barriers. A surface that can provide continual droplet-free areas for nucleation is favorable for condensation water harvesting. Here, we report a flow-separation condensation mode on a hydrophilic reentrant slippery liquid-infused porous surface (SLIPS) that rapidly removes droplets with diameters above 50 μm. The slippery reentrant channels lock the liquid columns inside and transport them to the end of each channel. We demonstrate that the liquid columns can harvest the droplets on top of the hydrophilic reentrant SLIPS at a high droplet removal frequency of 130 Hz/mm^2. The sustainable flow separation without flooding increases the water harvesting rate by 110% compared to the state-of-the-art hydrophilic flat SLIPS. Such a flow-separation condensation approach paves a way for water harvesting.

reentrant SLIPS | flow separation | condensation | heat transfer | water harvesting

Significance

Water harvesting from air has the potential to alleviate water scarcity in arid regions around the globe. To achieve efficient water harvesting, we prefer rapid vapor condensation and droplet collection simultaneously. Prior techniques are not able to separate the vapor and liquid flow, so the condensed droplets always hinder the vapor condensation. In this work, we report a flow-separation condensation mode on a hydrophilic reentrant slippery liquid-infused porous surface. The slippery reentrant channels absorb the condensed droplets, lock the liquid columns inside, and transport them to the end of each channel. As a result, the sustainable flow separation significantly increases the water harvesting rate.

Condensation is a common phase-change phenomenon that is widely used in water harvesting (1–5). Dropwise condensation can form discrete droplets on a low-surface-energy substrate and promote the heat transfer coefficient up to 10 times higher than filmwise condensation due to the rapid removal of condensates (6, 7). However, the displacement of air inside the structures can lead to a higher pinning force on the droplets, resulting in flooding on the superhydrophobic surface (8, 9). By replacing the air trapped inside the surface structures with liquid lubricant, researchers developed the slippery liquid-infused porous surface (SLIPS) to further promote heat transfer performance (1, 10–13). When condensed droplets grow to a certain diameter, they shed off a vertical surface due to the negligible contact angle hysteresis (12). To accelerate the droplet removal, directional droplet movements were developed to regulate the removal of water droplets on SLIPS (2, 5). However, these surfaces rely on gravity to remove large droplets that remain on the surface as thermal barriers before shedding during condensation.

Therefore, surfaces with partially hydrophilic and partially hydrophobic domains were developed to remove droplets from the condensing surface to the structures underneath. Such an amphiphilic surface has a hydrophobic top with a hydrophilic porous structure underneath (14, 15). During the condensation, droplets on the hydrophobic top are absorbed by the wetted hydrophilic structures underneath. However, the liquid film within the hydrophilic structures leads to partial or complete flooding at elevated heat fluxes due to the high pinning forces (9, 16, 17). Unlike the radiative cooling-induced dew harvesting in nature, droplets are directly condensed on the reentrant SLIPS by conduction and convection (18), where condensed droplets act as thermal barriers (19–21). Based on the condensation models (6, 22–24), each droplet contributes to the total thermal resistance, while smaller droplets have a lower thermal resistance. When a surface is only covered by small droplets (e.g., at the beginning of the condensation), the heat transfer coefficient is higher than that of a surface with larger droplets (25). Thus, rapid droplet nucleation and removal are desired to achieve a high heat transfer coefficient. Microchannels are applied to transport condensates as the flow resistances can be much smaller than those of micropillars. Hydrophilic slippery channels with or without biphilic coatings are used to enhance water harvesting, but they failed to separate the vapor and liquid as droplets emerged out of the channels or completely wetted the surfaces (1, 26–28). To suppress condensates from emerging out of the channel, the liquid column must be locked inside. The reentrant channels show a potential to lock the liquid inside due to their overhang structures. With a surface engineering approach, the reentrant structure has been modified to keep highly nonwetting liquids inside (29). However, the reentrant structures are wetted by liquids during condensation as the condensates are pinned inside the channels (30). Thus, the surface will transition to a complete wetting state at elevated heat fluxes.

Author affiliations: [a]Department of Mechanical Engineering, The University of Texas at Dallas, Richardson, TX 75080

Author contributions: Z.G. and X.D. designed research; Z.G., D.B., and X.D. performed research; Z.G., D.B., L.S., and X.D. analyzed data; and Z.G., D.B., L.S., and X.D. wrote the paper.

The authors declare no competing interest.

This article is a PNAS Direct Submission.

[1]To whom correspondence may be addressed. Email: Dai@utdallas.edu.

This article contains supporting information online at http://www.pnas.org/lookup/suppl/doi:10.1073/pnas.2209662119/-/DCSupplemental.

Published August 29, 2022.

To address those challenges, on a hydrophilic reentrant SLIPS, we present a flow-separation condensation mode that sustains rapid droplet removal on top and transports liquid columns underneath. Our approach is to make reentrant channels with hydrophilic and slippery boundary lubrication. Once droplets are condensed on the top hydrophilic slippery surface, they are removed immediately to the reentrant channels underneath, resulting in sustainable flow separation. Such a new condensation mode could significantly reduce the thermal resistance by rapidly removing droplets with diameters above 50 μm, leading to an exceptional water harvesting rate. This work not only proposes a flow separation approach to enhance water harvesting but also provides a universal concept to design surfaces for condensation heat transfer.

Results

Flow Separation: Vapor Condenses on the Top and Liquid Flows at the Bottom. Our experiments were carried out on a hydrophilic reentrant SLIPS with hydroxy-terminated polydimethylsiloxane (HPDMS) as the liquid lubricant (Fig. 1*A* and *SI Appendix*, Figs. S1–S3 and Table S1). We used solid fraction (Φ), surface roughness (R), and channel cross-section area (A) to name the substrates in this study (see details in *SI Appendix*, section S1). If not specified, the reentrant SLIPS used in this study has $\Phi = 0.66$ and $R = 3$. The samples were installed on a vertical cooling plate inside a humid chamber and maintained at 4 °C for water condensation. When the water droplet is condensed on the top of a hydrophilic reentrant SLIPS, an oil meniscus forms surrounding the droplet due to the balance of interfacial tension forces (5, 31). The nucleated droplets coalesce with each other due to the meniscus-mediated movement, i.e., coarsening effect (5) (*SI Appendix*, Fig. S4). Once the oil meniscus surrounding the water droplet on top of the reentrant surface contacts the liquid column inside the reentrant channel, the water droplet moves spontaneously from the top surface into the channel (Fig. 1 *A* and *B*, *SI Appendix*, Fig. S4, and Movie S1). The liquid column inside the reentrant channel is initially formed by direct vapor condensation. At the beginning of condensation, i.e., before the liquid column forms inside the reentrant channels, the vapor is condensed both inside the reentrant channels and on top of the reentrant surfaces (plateau zones) (*SI Appendix*, Fig. S5). Vapor condensation is faster on the top of the reentrant surfaces due to the edge effect (32, 33). As a result, we see a larger number of droplets on top of the reentrant SLIPS than those in the reentrant channels (*SI Appendix*, Fig. S5). In the steady-state condensation, the liquid columns in the reentrant channels come from the removed droplets from the plateau zones of the reentrant SLIPS. Even though the water molecules could condense and be absorbed by the liquid column (11, 34), the condensation of vapor is limited due to a larger thermal barrier than that of the condensate-free plateau zones (16). Thus, the condensation in the reentrant channel is negligible compared with that on top of the reentrant surfaces. The condensed droplets are absorbed by the channels due to the lower pressure of the liquid column (*SI Appendix*, Fig. S6). Thus, water

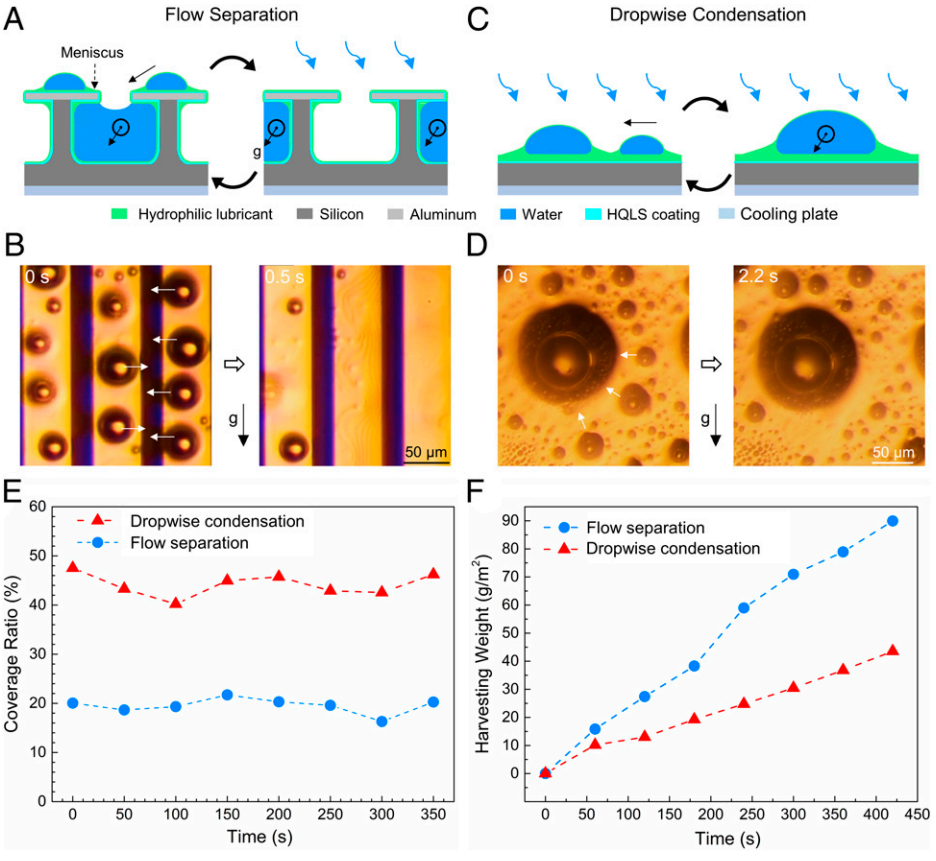

Fig. 1. Flow separation on hydrophilic reentrant SLIPS. (*A*) Schematic of flow separation. The small droplets move into the reentrant channels due to coarsening effect. Meanwhile, the liquid columns inside each reentrant channel slide due to gravity. The arrows show the moving direction of smaller droplets. (*B*) Microscope images of the flow separation. The white arrows show that smaller droplets move toward the reentrant channels. Droplets are removed from the surface. (*C*) Schematic of dropwise condensation with coarsening droplet on a slippery flat surface. The small droplet climbs on the oil meniscus and coalesces with a larger one. (*D*) Microscope images of the coarsening droplets. The arrows show the moving direction of smaller droplets. (*E*) The coverage ratios of surfaces with flow separation and dropwise condensation in the steady state. (*F*) The water harvesting weights from surfaces with flow separation and dropwise condensation.

vapor is condensed on the top of reentrant surfaces and liquid is collected by the bottom reentrant channels, forming flow separation.

The flow separation on hydrophilic reentrant SLIPS is different from the coarsening effect on hydrophilic flat SLIPS, where the oil meniscus surrounding a smaller water droplet contacts the oil meniscus surrounding a larger one (Fig. 1 *C* and *D* and Movie S1). Before the direct contact of the two droplets on hydrophilic SLIPS, the smaller droplet climbs spontaneously on the oil meniscus of the larger droplet, which results in a faster droplet coalescence than that on hydrophobic SLIPS (5, 35). Tiny droplets with diameters from 10 to 400 μm move toward larger droplets from all directions regardless of the surface orientation and coalesce immediately when they are in contact (<0.1 s). However, the coalesced droplets are pinned on the surface before they reach the shedding diameter at around 1,000 μm. The large droplets on the surface hinder further vapor condensation, while the hydrophilic reentrant SLIPS shows no droplet with a diameter above 50 μm.

Due to the flow separation, the condensed water droplets are rapidly removed into the slippery reentrant channels, which also transport the water columns to the end of each channel (*SI Appendix*, Fig. S7*A* and Movie S2). Moreover, no droplet emerges from the reentrant channels. In contrast, on a flat SLIPS with coarsening effect, big droplets must be removed from the surface by gravity (*SI Appendix*, Fig. S7*B* and Movie S2). To elucidate the significance of rapid droplet removal and transport, we measured the water coverage ratio φ (i.e., the percentage of the surface area covered by droplets) on reentrant and flat SLIPS in a steady state (Fig. 1*E* and *SI Appendix*, Fig. S8). The water coverage ratio of hydrophilic reentrant SLIPS is maintained at around 20%. However, on hydrophilic flat SLIPS large droplets are pinned on the surface before reaching the shedding diameter. Therefore, the water coverage ratio is 45% on hydrophilic flat SLIPS, which is more than two times compared to that on hydrophilic reentrant SLIPS. We further investigated the droplet removal frequency, f, which measures the number of removed droplets during a unit time in a fixed area (*SI Appendix*, Fig. S9). Due to the flow separation, the removal frequency is 130 Hz/mm^2, which is 440% higher than the 24 Hz/mm^2 on hydrophilic flat SLIPS. A higher removal frequency rapidly refreshes surfaces and provides more areas for nucleation. In addition, the low coverage ratio maintains a large area for nucleation, but this cannot be sustained on regular channel SLIPS once droplets emerge out of the channels.

We further measured the water harvesting weight of each surface with time (Fig. 1*F* and Movies S2 and S3). During condensation, the droplet volume increases linearly with time for both flow separation and dropwise condensation. Due to the flow separation-induced rapid droplet removal, more liquids can be transported to the bottom of the hydrophilic reentrant SLIPS than those on hydrophilic flat SLIPS. The random movement of tiny droplets on hydrophilic flat SLIPS results in a low growth rate of large droplets. In contrast, flow separation on hydrophilic reentrant SLIPS rapidly removes droplets into the slippery reentrant channels, giving rise to a larger water harvesting weight. A greater amount of heat transfer is proportional to a larger amount of latent heat for an increased liquid mass generation. Thus, the enhancement of the water harvesting rate is linearly proportional to the enhancement of heat flux. As a result, the flow separation on hydrophilic reentrant SLIPS shows a 115% higher water harvesting weight than dropwise condensation on hydrophilic flat SLIPS due to the higher removal frequency and lower coverage ratio.

Flow Separation Enables Rapid Droplet Size Evolution. The flow separation gives rise to a rapid droplet size evolution on the hydrophilic reentrant SLIPS. In this work, we define droplets with diameters below 50 μm as "tiny" droplets. We measured the droplet size distributions in the middle and at the bottom of the surface, respectively. Flow separation removes droplets from the reentrant surfaces into the reentrant channels. The removed droplets transport through the reentrant channels to the bottom and provide a large water-free area for further condensation (Fig. 2*A* and Movie S4). Thus, the flow separation leads to a rapid droplet size evolution over time on the surface (Fig. 2 *B* and *C* and Movie S3). The number of tiny droplets varies slightly due to the continual flow-separation condensation. On the contrary, the hydrophilic flat SLIPS relies on shedding droplets to remove condensates from the surface (Fig. 2*D* and Movies S2 and S3). Thus, the droplet size distribution at the bottom evolves slowly from 300 s to 350 s (Fig. 2 *E* and *F*). Even though the coarsening effect could increase the water harvesting rate, large droplets are pinned on the surface before shedding. Thus, the overall evolution of droplet size distribution on hydrophilic flat SLIPS is slower than that on the hydrophilic reentrant SLIPS.

Based on previous dropwise condensation models, a surface with tiny droplets (25) and a rapid size evolution (5) shows a desirable heat-transfer coefficient. At the beginning of the condensation, surfaces show a higher heat-transfer coefficient due to the dense distribution of tiny droplets (25). Meanwhile, a rapid droplet size evolution shows the rapid removal of droplets, which can provide more droplet-free areas for nucleation (5). Thus, we have achieved rapid water harvesting due to the flow-separation condensation, which outperforms dropwise condensation.

Design Rationale to Achieve Flow Separation. To achieve flow separation for rapid droplet removal, there are two key parameters: 1) hydrophilic slippery interface and 2) reentrant channel. We infused HPDMS on a hydrophilic quasi-liquid surface-coated reentrant structure to achieve a hydrophilic slippery interface (Fig. 3*A* and *SI Appendix*, Fig. S10). The hydrophilic lubricant also enables a meniscus-mediated coarsening effect to remove tiny droplets (5). Due to the coarsening effect, droplets on top of the hydrophilic reentrant SLIPS move spontaneously without direct contact with the liquid column inside the reentrant channel (Fig. 3*B* and Movie S5). We also studied the droplet dynamics on a hydrophilic bare reentrant surface, which showed a high pinning force for water droplets (*SI Appendix*, Fig. S11). When droplets on the hydrophilic bare surface directly contacted the liquid inside the channel, they were absorbed into the wetted channel due to the capillary force (9), but there was water residue on the reentrant surfaces due to the high pinning, leading to a partial flow separation (Fig. 3 *C* and *D*). On the contrary, droplets on the hydrophobic reentrant SLIPS with silicone oil lubricant could not move into the channel. Instead of being absorbed by the hydrophobic reentrant channel, droplets coalesced with each other and showed nonwetting on the top of the hydrophobic reentrant SLIPS (Fig. 3 *E* and *F*). Thus, the hydrophilic interface is required to remove the droplets into the reentrant channels. Furthermore, the reentrant channels must have boundary lubrication to remove the liquid columns, which enables liquid columns to slide along with the gravity inside the reentrant channels with a slippery interface (Fig. 3*G*, *SI Appendix*, Fig. S12, and Movie S6). However, the hydrophilic bare reentrant surface shows wetted channels with pinned liquid columns (Fig. 3*H*). Eventually, the hydrophilic reentrant SLIPS collected numerous

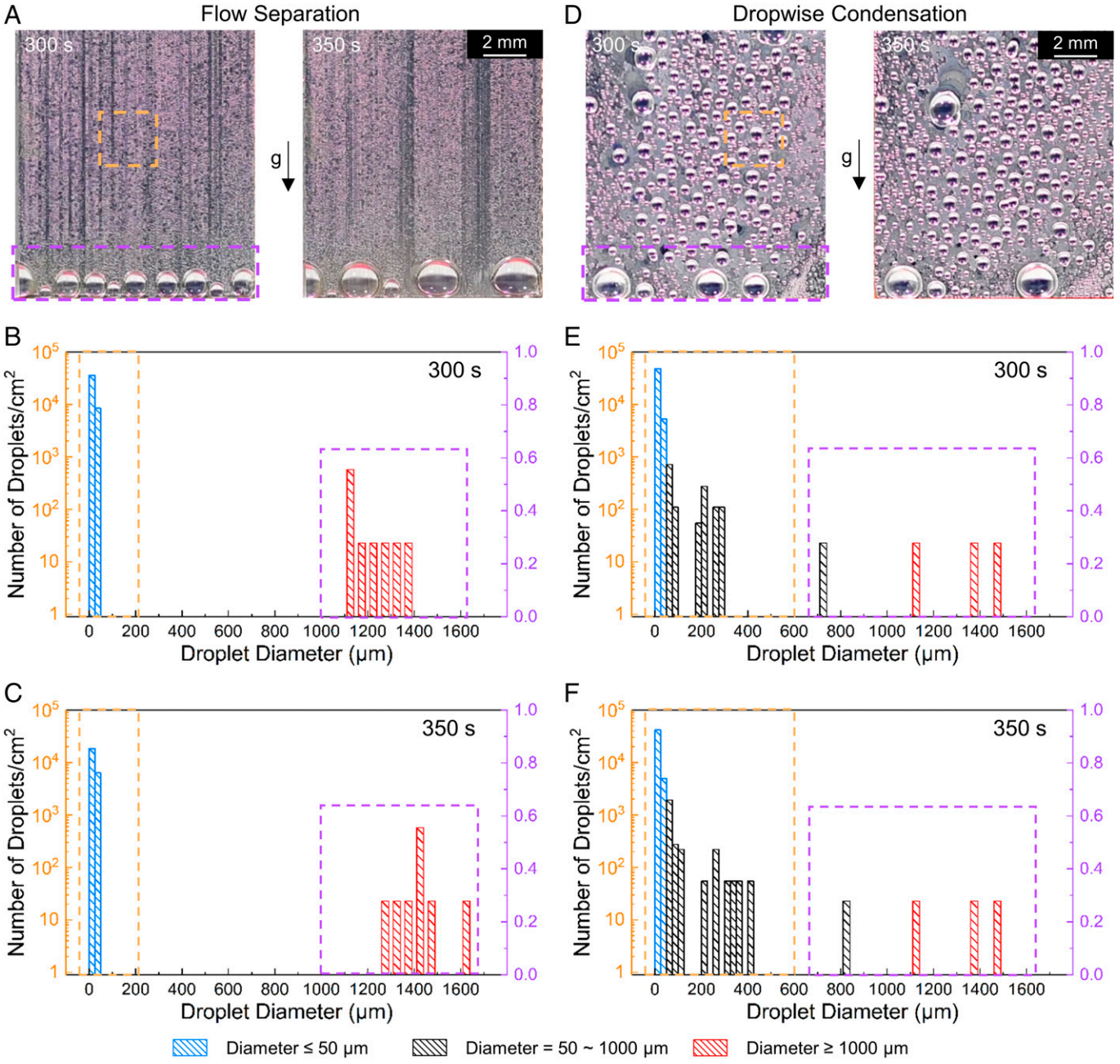

Fig. 2. Droplet size distribution of flow separation and coarsening droplets. (*A*) Microscope images of droplets on a flow separation surface during water harvesting. Only large droplets can be observed at the bottom. (Scale bar, 2 mm.) Droplet size distribution of flow separation at 300 s (*B*) and 350 s (*C*) after the first nucleation. It shows the flow separation-induced rapid evolution of droplet size with time. (*D*) Microscope images of droplets on a coarsening droplet surface during water harvesting. Droplets are densely distributed on the surface. (Scale bar, 2 mm.) Droplet size distribution of coarsening droplet at 300 s (*E*) and 350 s (*F*) after the first nucleation. Orange square shows the droplet size distribution in the middle of the surface. Purple square shows the droplet size distribution at the bottom of the surface. All *y* axes show the number of droplets per square centimeter.

droplets at the bottom of the surface while the hydrophilic bare reentrant surface showed a liquid film (*SI Appendix*, Fig. S13 and Movie S7). We quantified the droplet volumes at the bottom of hydrophilic reentrant SLIPS, hydrophobic reentrant SLIPS, and hydrophilic bare reentrant surface as 5.5, 1.1, and 0 μL, respectively (Fig. 3*I* and Movie S7). Moreover, the coverage ratio on hydrophobic reentrant SLIPS is 2.2 times higher than that on hydrophilic reentrant SLIPS (*SI Appendix*, Fig. S14). This further shows a hydrophilic slippery interface is essential to achieve flow separation.

To elucidate the enhancement of the coarsening effect, we studied the droplet dynamics on a hydrophilic surface with a low contact angle hysteresis (<3.8°) [i.e., PEGylated coated surface (36)]. As the PEGylated polymer cannot be coated on the top aluminum of reentrant channels, we used regular channels to show a hydrophilic slippery surface without the coarsening effect. Like the bare hydrophilic surface, the PEGylated channels show a partial separation (*SI Appendix*, Fig. S15). Due to the slippery interface, droplets are absorbed by the channel, leaving no residue. Meanwhile, the slippery channels transport liquid columns to the bottom of the surface, but a large number of droplets remain on the surface until direct contact with the wetted channels. The coverage ratio on PEGylated channels is larger than that on hydrophilic reentrant SLIPS. To achieve flow separation on the reentrant channels, the surface should be a hydrophilic SLIPS with coarsening effect.

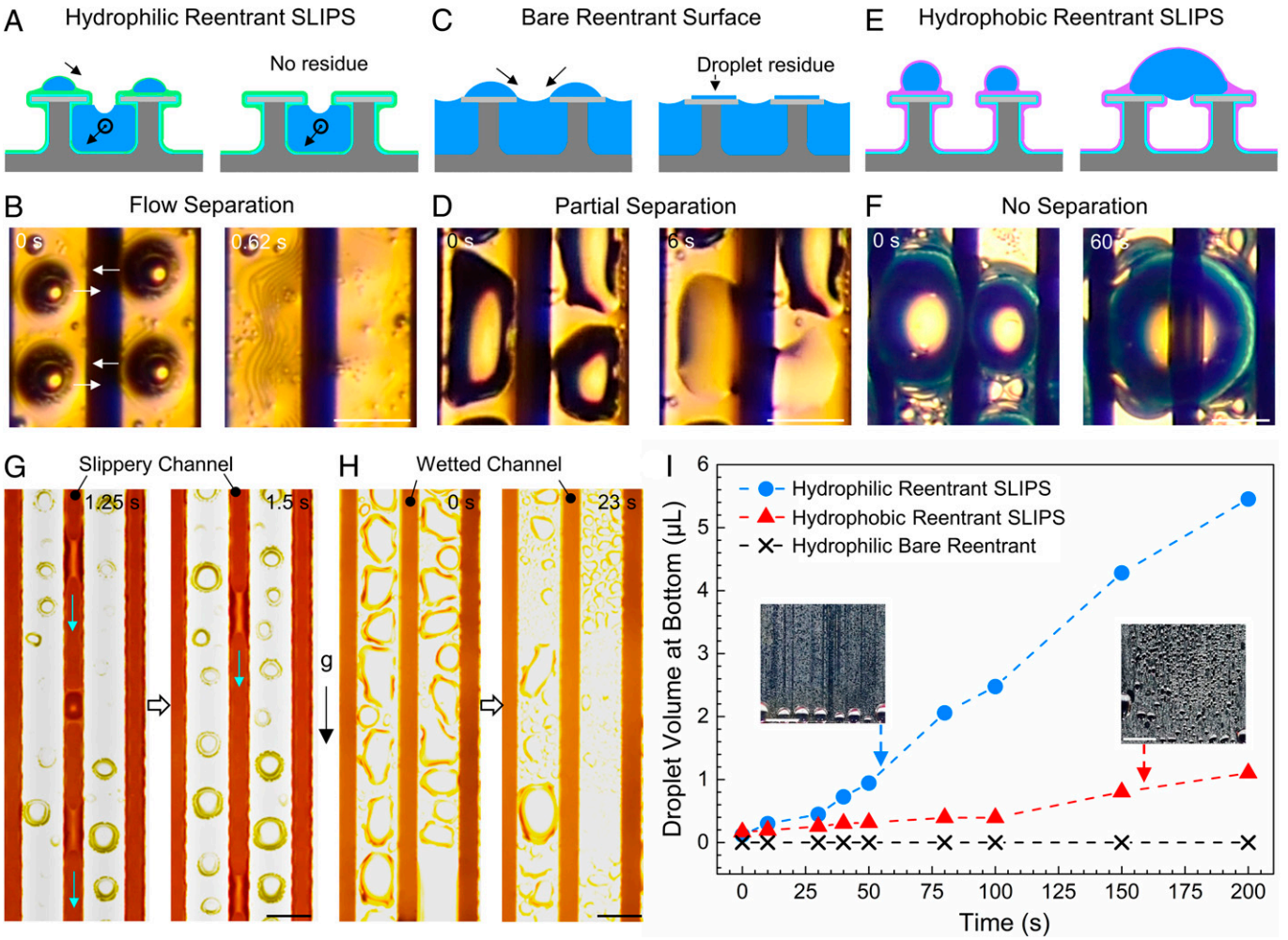

Fig. 3. Hydrophilic reentrant SLIPS enables flow separation. Schematic (*A*) and microscope view (*B*) of droplet movement on a hydrophilic reentrant SLIPS during water harvesting. Droplets move to the channel due to the meniscus-mediated coarsening effect. Schematic (*C*) and microscope view (*D*) of droplet movement on hydrophilic bare reentrant channels. Droplets are removed into the channel by direct contact. Schematic (*E*) and microscope view (*F*) of droplet movement on a hydrophobic reentrant SLIPS. Droplets pin on top of the surface after droplet coalescence. (*G*) Liquid shedding inside slippery channels of hydrophilic reentrant SLIPS. The green arrows show the movement direction. (*H*) Liquid wetting inside hydrophilic channels. The liquid column has no movement. (Scale bars in *B, D, F, G*, and *H*, 50 μm.) (*I*) Droplet volume collected at the bottom of the surface varies with the surface modification. (*Insets*) The overall performances during water harvesting experiments after 200 s of first droplet formation. (Scale bar, 5 mm.)

Hydrophilic Reentrant SLIPS Locks the Liquid Column to Sustain Flow Separation. To achieve a complete flow separation, the reentrant geometry is critical to locking the liquid inside the reentrant channels and preventing droplets from emerging out (Fig. 4 *A*–*D*). To show the difference between the reentrant channels from regular channels, we fixed the pitch width of the channel top as 50 μm but varied the interchannel spacing and height for both the reentrant and regular channels (*SI Appendix*, Fig. S16). During condensation, the liquid column grows by absorbing droplets from the top of the regular channel SLIPS. With the increased volume, the energy balance of the liquid column changes the interface curvature and generates the Laplace pressure as a driven force. Thus, the liquid column can have two movement directions, including 1) emergence outside the channel and 2) elongation along the channel. On hydrophilic reentrant SLIPS, there is only liquid column elongation without emergence (Fig. 4*A*). The liquid columns transport inside the reentrant channels to the end of each channel (Fig. 4*B*). However, on the hydrophilic channel SLIPS the liquid columns show both elongation and emergence, where the emergences of the liquid droplets are dominating on the surface (Fig. 4 *C* and *D*).

The hydrophilic reentrant SLIPS provides a higher pinning force along the emergence direction, which is generated by the overhangs of reentrant structures (Fig. 4*E* and *SI Appendix*, Fig. S17). The pinning force at the corner of the reentrant overhang is higher than that in the regular channel. This results from the three-phase contact line movement across the discontinuous geometry (i.e., horizontal overhang to vertical wall) (29, 37, 38). To emerge out of the reentrant channels, the contact line first moves horizontally underneath the overhang then moves vertically on the side wall of the overhang (*SI Appendix*, Fig. S17). The discontinuous geometry of the reentrant structure changes the contact line movement direction and increases the pinning force (38–40). The liquid column will emerge out of the reentrant channel when its contact angle increases from the equilibrium contact angle (θ_e) to the advancing angle (θ_{adv}), (Fig. 4*E* and *SI Appendix*, Fig. S17). Thus, we calculated the energy barrier due to pinning force along the emergence direction E_p as

$$E_p = 2\gamma(\cos\theta_e - \cos\theta_{adv}) \cdot L \cdot dH, \quad [1]$$

where γ is the surface tension of the condensed liquid, L is the length of the liquid column, and dH is the increased height of the liquid column. The liquid column inside a regular channel

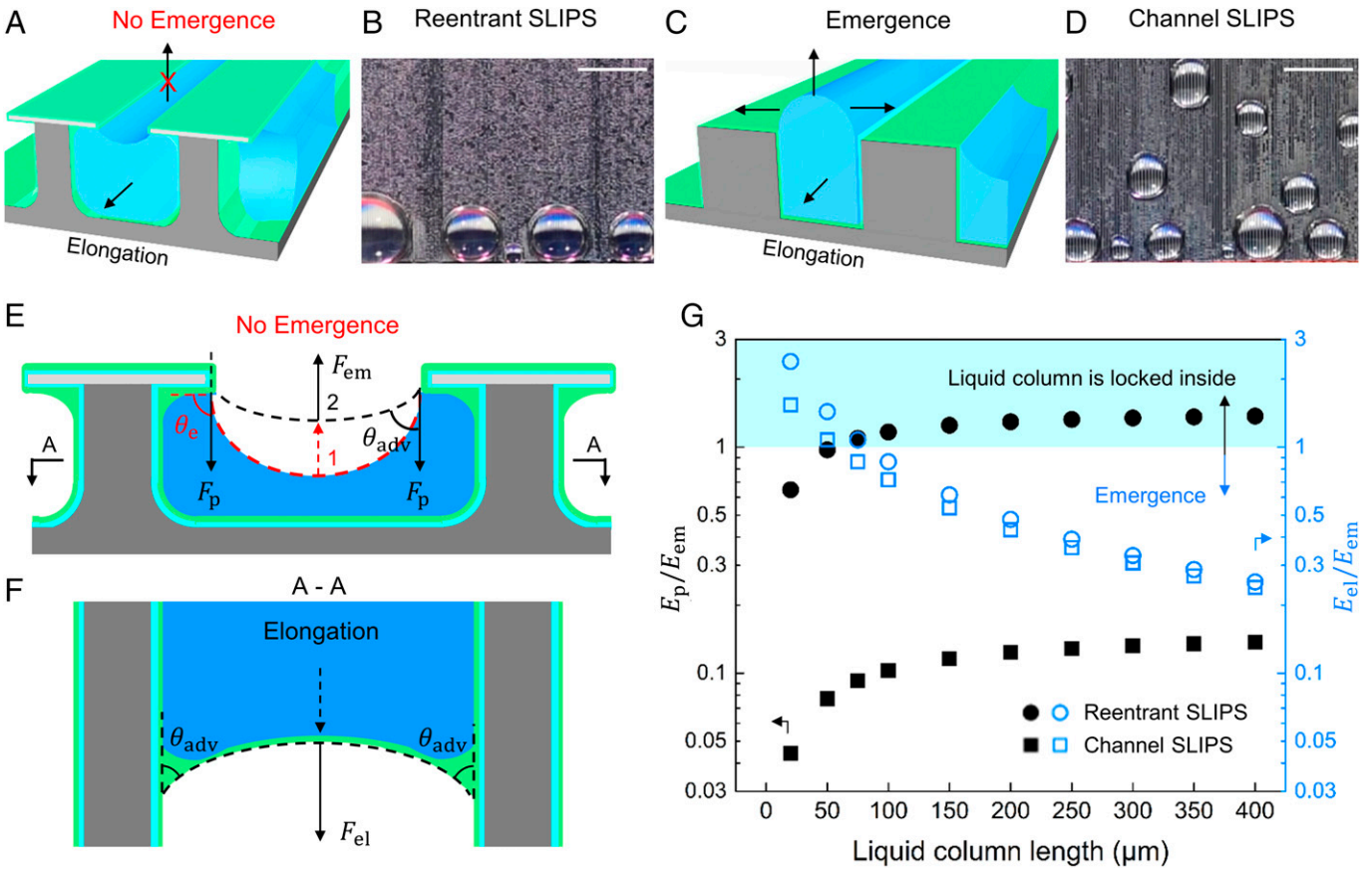

Fig. 4. Hydrophilic reentrant SLIPS locks liquid columns. (*A*) Three-dimensional schematic of hydrophilic reentrant SLIPS with locked liquid column. (*B*) Hydrophilic reentrant SLIPS has only large droplets at the bottom during condensation. (Scale bar, 2.5 mm.) (*C*) Three-dimensional schematic of the slippery regular channel SLIPS with an emerging liquid column. (*D*) Regular channel SLIPS covered with droplets during condensation. (Scale bar, 2.5 mm.) (*E*) Cross-section of water column inside the slippery reentrant SLIPS. No liquid emergence due to a high pinning force F_p of the discontinuous geometry. The emergence energy $E_{em} \sim F_{em} A_{em}$. (*F*) Schematic of liquid column elongation from A-A section of reentrant SLIPS. (*G*) A larger energy barrier to overcome the pinning energy (E_p) than the emergence energy (E_{em}) prevents the liquid column from emerging out of the reentrant SLIPS. The energy ratio of elongation energy (E_{el}) and emergence energy (E_{em}) shows the droplet movement based on the length of the liquid column. The cross-sectional area of each reentrant and channel SLIPS is 2,500 μm^2.

advances only on the sidewall of the channel, which has a smaller pinning force than the reentrant channel (*SI Appendix*, Fig. S17). To further investigate the movement of the liquid column, we built a model with an energy analysis to predict the emergence and elongation (Fig. 4 *E* and *F* and *SI Appendix*, Figs. S17 and S18) (16). The emergence energy of Laplace pressure E_{em} is

$$E_{em} = \Delta P_{em} \cdot A_{em} \cdot dH, \quad [2]$$

where ΔP_{em} is the Laplace pressure at the interface of emergence and A_{em} is the top surface area of the liquid column. Similarly, the elongation energy of Laplace pressure E_{el} is (Fig. 4*F* and *SI Appendix*, Fig. S18)

$$E_{el} = \Delta P_{el} \cdot A_{el} \cdot dL, \quad [3]$$

where ΔP_{el} is the Laplace pressure at the interface of elongation, A_{el} is the cross-section area of the liquid column along the channel, and dL is the elongated length of the liquid column. We compared the energy of the reentrant channel and the regular channel with the same channel height and cross-section area (Fig. 4*G* and *SI Appendix*, Fig. S19). The liquid column will emerge when the emergence energy is larger than the elongation energy (i.e., $E_{em} > E_{el}$; Fig. 4*G* and *SI Appendix*, Fig S19). With the increased length of the liquid column inside the channel, the liquid column will prefer to emerge out of the channel instead of elongating along the channel. In the reentrant channel, $E_p > E_{em}$ shows the droplet has no emergence. However, the droplet in a regular channel tends to emerge as $E_p < E_{em}$, which is the result of a smaller pinning force on the sidewall of the regular channel compared with the reentrant channel. The retention force F_r along the liquid column elongation is much smaller than the elongation force due to a small contact angle hysteresis (≤1°), which has a limited effect on liquid column emergence and elongation. Meanwhile, a smaller solid fraction has a larger ratio of E_{em}/E_{el}, which is easier to emerge than elongate. A deeper regular channel with a smaller solid fraction can delay the emergence of the liquid column but cannot prevent it (*SI Appendix*, Figs. S16, S19, and S20). The energy model is further validated by condensation in both vertical and horizontal orientations, respectively (*SI Appendix*, Figs. S20 and S21). On horizontal surfaces, droplets only grow at the ends of each reentrant channel on hydrophilic reentrant SLIPS, while droplets grow out of the channels on hydrophilic channel SLIPS. The reentrant structure shows a significant advantage over the rectangular channel (*SI Appendix*, Fig. S22). An increased height of liquid column will increase the energy ratio between elongation and emergence, where reentrant SLIPS needs a smaller height to prevent emergence than channel SLIPS. Only the reentrant structure can prevent droplet emergence due to the large pinning force in the emergence direction. By increasing the lubricant thickness, i.e., surfaces are entirely coated with the liquid lubricant, the overhangs will be filled with lubricant (*SI Appendix*, Fig. S23). In this case, the liquid column can emerge out of the reentrant channel and form droplets as

there is no discontinuous geometry. The reentrant overhang locks the liquid column and forces it to elongate instead of emerging. An optimized hydrophilic reentrant SLIPS may achieve a complete flow separation to enable rapid droplet removal and transport at varying heat fluxes.

Flow Separation Enhances Water Harvesting. We quantified the water harvesting rates on three surfaces with/without flow separation (Fig. 5*A* and Movie S8). Hydrophilic reentrant SLIPS shows no droplet out of the reentrant channels, while other surfaces have droplet emergence out of the channels. Hydrophilic channel SLIPS ($\Phi = 0.5$ and $R = 2$) shows the largest coverage ratio, which is 220% higher than that on hydrophilic reentrant SLIPS ($\Phi = 0.66$ and $R = 3$). The hydrophilic channel SLIPS shows the lowest removal frequency, which is 60% of that of hydrophilic reentrant SLIPS. The emerging droplets occupy a large surface area on top, so the removal frequency is reduced due to a larger coverage ratio. With emerging droplets, the droplet removal shows a mixed mode of partial separation and shedding. Instead of sliding inside the channels, droplets emerge out and shed off due to gravity once they reach the shedding diameter. Even though the hydrophilic channel SLIPS has emerging droplets, the removal frequency is increased by partial flow separation, which is more than 200% higher than that of the hydrophilic flat SLIPS (Fig. 5*A*).

We quantified the water harvesting rates on hydrophilic reentrant SLIPS, hydrophilic channel SLIPS, and hydrophilic flat SLIPS (Fig. 5*B*, *SI Appendix*, Fig. S24, and Movie S9). Hydrophilic reentrant SLIPS shows a complete flow separation and achieves the highest water harvesting rate of 13.7 $g{\cdot}m^{-2}{\cdot}min^{-1}$, which is 110% higher than that of hydrophilic flat SLIPS. On hydrophilic channel SLIPS (e.g., $\Phi = 0.66$ and $R = 2.3$), the droplet dynamics mode is partial separation with shedding droplets above the channels. Thus, the water harvesting rate is only 67% of the hydrophilic reentrant SLIPS but is still 39% higher than that of hydrophilic flat SLIPS (*SI Appendix*, Fig. S24). A larger energy ratio between pinning force and emergence energy shows a higher harvesting rate, which is due to the locking of the liquid column. With the presence of the reentrant structure, increasing the channel height will favor the flow separation due to the increased elongation energy. Note that the optimized geometry is also related to heat flux. A higher heat flux needs larger reentrant channels to transport all condensates to avoid surface flooding. Compared with the coarsening-enhanced shedding droplets, the flow separation can rapidly remove droplets with diameters above 50 μm, and the liquid columns are locked inside and transported to the end of each channel. The flow-separation condensation mode provides a large droplet-free area and significantly reduces the thermal resistance during condensation. Thus, hydrophilic reentrant SLIPS achieves a higher water harvesting rate than hydrophilic channel SLIPS and hydrophilic flat SLIPS. However, the reentrant SLIPS suffers from durability issues due to the loss of lubricant by droplet depletion. In this work, we focused on the dew harvesting test to show the physics of the flow separation process. This fundamental study will help people to design a durable flow-separation surface in the future. The collected water with oil content will be purified by using a water–oil separation film (41, 42). Creating a durable condensation surface is an emerging research direction in this area. For instance, the quasi-liquid surfaces have the potential to address the durability issue of lubricant depletion (43).

Discussion

We reported a flow-separation condensation mode to rapidly harvest condensed droplets from hydrophilic reentrant SLIPS. The flow separation uses the slippery interface to move the droplets with diameters above 50 μm into the reentrant channels, providing a large droplet-free area for further vapor condensation. To sustain the flow separation, a hydrophilic and slippery reentrant channel is required to absorb the condensed droplets. Moreover, the overhangs lock the liquid columns inside and direct them to the end of each reentrant channel. No droplet emerges out of the reentrant channels on hydrophilic reentrant SLIPS due to the high energy barrier of the reentrant geometry. This prevents large droplet formation and surface flooding during condensation. The flow separation on hydrophilic reentrant SLIPS sustains a water coverage ratio down to 20% and a droplet removal frequency of 130 Hz/mm^2. As a result, the water harvesting rate is 110% higher than that on hydrophilic flat SLIPS. This work not only

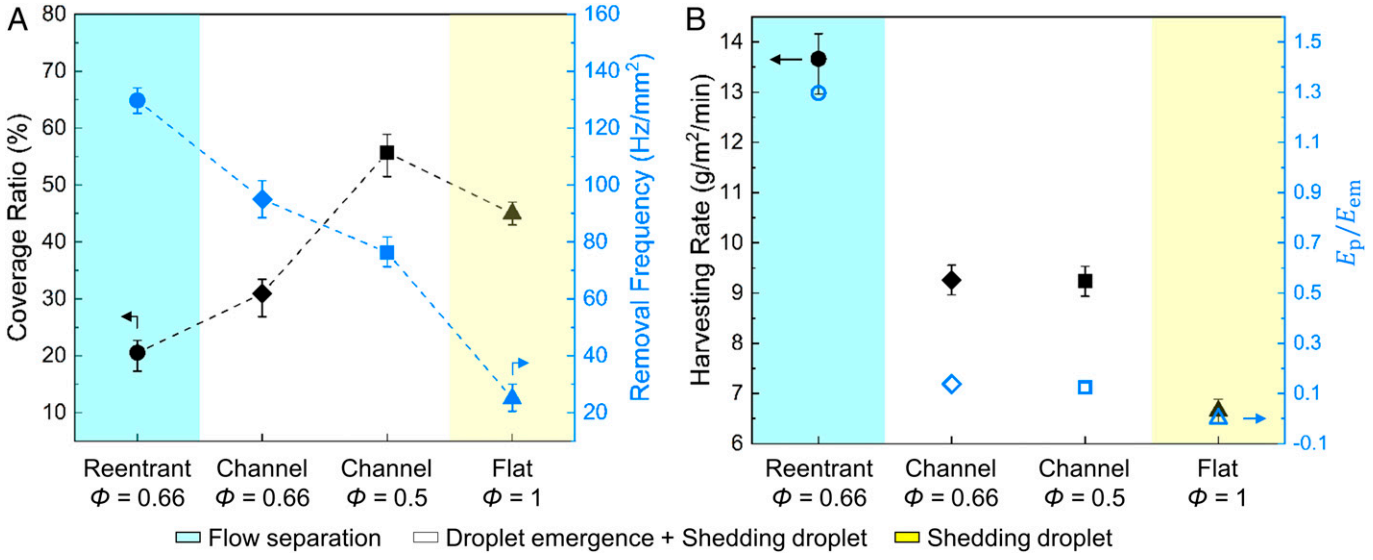

Fig. 5. Water harvesting on hydrophilic reentrant SLIPS, hydrophilic channel SLIPS, and hydrophilic flat SLIPS. (*A*) Coverage ratio and droplet removal frequency on hydrophilic reentrant SLIPS and hydrophilic channel SLIPS. (*B*) Water harvesting rate and the ratio of pinning and emergence energy. Hydrophilic reentrant SLIPS shows flow separation with the highest water harvesting rate and energy ratio. The error bars are from the measurement uncertainties.

demonstrates a sustainable flow-separation mode for improving water harvesting but also provides a paradigm beyond dropwise condensation for water and energy sustainability.

Materials and Methods

Water Harvesting Experiments. The dew harvesting tests were performed in a self-built closed chamber at atmospheric pressure (1 atm) (5). The chamber was made of plastic slides with a glass in the front. The plastic slides were assembled with a sealant. An aluminum cooling plate was attached to the plastic slide vertically with double-sided tape and the temperature of the cooling plate was controlled by a recirculation chiller with deionized (DI) water as the coolant. The humidity inside the chamber was maintained at 95 ± 3% by a humidifier and was measured by a humidity meter (Cole-Parmer). The water vapor temperature was room temperature 22 °C and the dew point was 20 °C. A thermocouple was attached to the sample surface and fixed with double-sided copper tape on the cooling stage. The sample temperature could vary from 4 °C to 18 °C, the same as the cooling plate temperature. The videos and images were captured using a Nikon digital camera assembled with a microscope. The sample was illuminated by a light-emitting diode ring light assembled with the microscope.

Fabrication of Reentrant Structure. The fabrication process of the reentrant structure (30, 38) is shown in *SI Appendix*, Fig. S1. First, a 4-inch silicon wafer (500-μm thickness, p-type, and <1 0 0>) was cleaned with acetone and DI water, successively. After drying with pure nitrogen gas, the silicon wafer was treated with 20 min of hexamethyldisilane (HMDS) adhesion process. Then, the silicon wafer was coated with negative photoresist nLoF 2020 with 1-min soft baking at 115 °C (*SI Appendix*, Fig. S1*A*). The coated wafer was exposed under i-line in an ultraviolet printer, followed by 1-min hard baking at 115 °C and developed by AZ 300 MIF developer (*SI Appendix*, Fig. S1*B*). Then, 50-nm-thick chromium (adhesion layer) and 1-μm-thick aluminum were deposited on a silicon wafer by an e-gun evaporator (*SI Appendix*, Fig. S1*C*). After done lift-off by AZ 400T stripper at 70 °C (*SI Appendix*, Fig. S1*D*), anisotropic etching of silicon was carried out via Plasma-Therm deep reactive ion etching (*SI Appendix*, Fig. S1*E*). Finally, the isotropic etching was carried out via March Asher PX-250 (*SI Appendix*, Fig. S1*F*). The flow rate for plasma cleaning was 17 sccm with 200-W power and 200-Torr pressure, and the flow rate of CF_4:O_2 for isotropic etching was 30:4 sccm with 200-W power and 100-Torr pressure. We used a scanning electron microscope to visualize the structures shown in *SI Appendix*, Fig. S1 *G* and *H*.

Surface Lubrication. The hydrophilic quasi-liquid surface (HQLS) and quasi-liquid surface (QLS) (44–46) were made by a one-step grafting method shown in *SI Appendix*, Fig. S3. First, the substrates (bare silicon or reentrant structure) were treated by plasma at ∼300 Torr for 25 min. For HQLS, the treated substrate was immersed into the HPDMS (average Mn ∼550, viscosity ∼25 cSt; Sigma-Aldrich) for 18 h at 50 °C on the hotplate. For QLS, the treated substrate was immersed into the silicone oil (20 cSt; Sigma-Aldrich) for 18 h at 50 °C on the hotplate. Then, the grafted substrates were cleaned with toluene, acetone, and DI water, successively, and dried by air. HQLS/QLS coating enables further lubricant infusion to form SLIPS. Then, the lubricants were spin-coated on the substrate with a spin speed of 4,000 rpm without any specification.

Contact Angle and Contact Angle Hysteresis Measurements. The measured contact angle and contact angle hysteresis on different substrates and lubricants are shown in *SI Appendix*, Table S1. For SLIPS surfaces, the spin speed is 4,000 rpm without any specification. The contact angle measurements and surface tension measurements were carried out using a standard goniometer (Model 290; Rame-hart) at room temperature under ambient conditions (20∼22 °C, ∼50% relative humidity). All the contact angle values were averaged from at least five independent measurements by applying 5-μL droplets on the samples.

Data, Materials, and Software Availability. All study data are included in the article and/or supporting information.

ACKNOWLEDGMENTS. Z.G., D.B., and X.D. gratefully acknowledge the Young Investigator Program at Army Research Office (Award W911NF1910416), the NSF Faculty Early Career Development Program (Award 2044348), and the Major Research Instrumentation Program (Award 2018188). L.S. was supported by the startup funds at the University of Texas at Dallas (UT Dallas). This project was partially funded by the Office of Research at UT Dallas through the Core Facility Voucher Program.

1. X. Dai *et al.*, Hydrophilic directional slippery rough surfaces for water harvesting. *Sci. Adv.* **4**, eaaq0919 (2018).
2. K.-C. Park *et al.*, Condensation on slippery asymmetric bumps. *Nature* **531**, 78–82 (2016).
3. Y. Hou, M. Yu, X. Chen, Z. Wang, S. Yao, Recurrent filmwise and dropwise condensation on a beetle mimetic surface. *ACS Nano* **9**, 71–81 (2015).
4. A. T. Paxson, J. L. Yagüe, K. K. Gleason, K. K. Varanasi, Stable dropwise condensation for enhancing heat transfer via the initiated chemical vapor deposition (iCVD) of grafted polymer films. *Adv. Mater.* **26**, 418–423 (2014).
5. Z. Guo, L. Zhang, D. Monga, H. A. Stone, X. Dai, Hydrophilic slippery surface enabled coarsening effect for rapid water harvesting. *Cell Rep. Phys. Sci.* **2**, 100387 (2021).
6. E. Le Fevre, J. Rose, An experimental study of heat transfer by dropwise condensation. *Int. J. Heat Mass Transf.* **8**, 1117–1133 (1965).
7. S. Kim, K. J. Kim, Dropwise condensation modeling suitable for superhydrophobic surfaces. *J. Heat Transfer* **133**, 081502 (2011).
8. R. Wen *et al.*, Hierarchical superhydrophobic surfaces with micropatterned nanowire arrays for high-efficiency jumping droplet condensation. *ACS Appl. Mater. Interfaces* **9**, 44911–44921 (2017).
9. C.-W. Lo, Y.-C. Chu, M.-H. Yen, M.-C. Lu, Enhancing condensation heat transfer on three-dimensional hybrid surfaces. *Joule* **3**, 2806–2823 (2019).
10. T.-S. Wong *et al.*, Bioinspired self-repairing slippery surfaces with pressure-stable omniphobicity. *Nature* **477**, 443–447 (2011).
11. R. Xiao, N. Miljkovic, R. Enright, E. N. Wang, Immersion condensation on oil-infused heterogeneous surfaces for enhanced heat transfer. *Sci. Rep.* **3**, 1988 (2013).
12. S. Anand, A. T. Paxson, R. Dhiman, J. D. Smith, K. K. Varanasi, Enhanced condensation on lubricant-impregnated nanotextured surfaces. *ACS Nano* **6**, 10122–10129 (2012).
13. D. Angelescu, T. Moscato, F. Pauchet, R. Van Kuijk, "Micro-structured surface having tailored wetting properties." US Patent 8,859,090 (2014).
14. D. M. Anderson *et al.*, Using amphiphilic nanostructures to enable long-range ensemble coalescence and surface rejuvenation in dropwise condensation. *ACS Nano* **6**, 3262–3268 (2012).
15. J. Oh *et al.*, Thin film condensation on nanostructured surfaces. *Adv. Funct. Mater.* **28**, 1707000 (2018).
16. R. L. Winter, M. McCarthy, Dewetting from amphiphilic minichannel surfaces during condensation. *ACS Appl. Mater. Interfaces* **12**, 7815–7825 (2020).
17. R. Wen *et al.*, Sustaining enhanced condensation on hierarchical mesh-covered surfaces. *Natl. Sci. Rev.* **5**, 878–887 (2018).
18. Z. Xu, L. Zhang, K. Wilke, E. N. Wang, Multiscale dynamic growth and energy transport of droplets during condensation. *Langmuir* **34**, 9085–9095 (2018).
19. D. Beysens, Dew nucleation and growth. *C. R. Phys.* **7**, 1082–1100 (2006).
20. D. Beysens, *Dew Water* (River Publishers, 2018), pp. 55–101.
21. D. Beysens, *The Physics of Dew, Breath Figures and Dropwise Condensation* (Springer, 2022), pp. 273–275.
22. E. Le Fevre, J. W. Rose, "A theory of heat transfer by dropwise condensation" in *Proceedings of the Third International Heat Transfer Conference* (Begel House Inc., Chicago, IL, 1966), pp. 362–375.
23. J. Rose, L. Glicksman, Dropwise condensation–The distribution of drop sizes. *Int. J. Heat Mass Transf.* **16**, 411–425 (1973).
24. P. B. Weisensee *et al.*, Condensate droplet size distribution on lubricant-infused surfaces. *Int. J. Heat Mass Transf.* **109**, 187–199 (2017).
25. S. Zheng, F. Eimann, C. Philipp, T. Fieback, U. Gross, Modeling of heat and mass transfer for dropwise condensation of moist air and the experimental validation. *Int. J. Heat Mass Transf.* **120**, 879–894 (2018).
26. R. D. Narhe, D. A. Beysens, Nucleation and growth on a superhydrophobic grooved surface. *Phys. Rev. Lett.* **93**, 076103 (2004).
27. P.-B. Bintein, H. Lhuissier, A. Mongruel, L. Royon, D. Beysens, Grooves accelerate dew shedding. *Phys. Rev. Lett.* **122**, 098005 (2019).
28. M. K. Chaudhury, A. Chakrabarti, T. Tibrewal, Coalescence of drops near a hydrophilic boundary leads to long range directed motion. *Extreme Mech. Lett.* **1**, 104–113 (2014).
29. K. L. Wilke, Z. Lu, Y. Song, E. N. Wang, Turning traditionally nonwetting surfaces wetting for even ultra-high surface energy liquids. *Proc. Natl. Acad. Sci. U.S.A.* **119**, e2109052119 (2022).
30. K. L. Wilke, D. J. Preston, Z. Lu, E. N. Wang, Toward condensation-resistant omniphobic surfaces. *ACS Nano* **12**, 11013–11021 (2018).
31. F. Schellenberger *et al.*, Direct observation of drops on slippery lubricant-infused surfaces. *Soft Matter* **11**, 7617–7626 (2015).
32. M.-G. Medici, A. Mongruel, L. Royon, D. Beysens, Edge effects on water droplet condensation. *Phys. Rev. E Stat. Nonlin. Soft Matter Phys.* **90**, 062403 (2014).
33. Y. Zhao *et al.*, Effects of millimetric geometric features on dropwise condensation under different vapor conditions. *Int. J. Heat Mass Transf.* **119**, 931–938 (2018).
34. S. Anand, K. Rykaczewski, S. B. Subramanyam, D. Beysens, K. K. Varanasi, How droplets nucleate and grow on liquids and liquid impregnated surfaces. *Soft Matter* **11**, 69–80 (2015).
35. J. Sun, P. B. Weisensee, Microdroplet self-propulsion during dropwise condensation on lubricant-infused surfaces. *Soft Matter* **15**, 4808–4817 (2019).
36. H. Cha *et al.*, Dropwise condensation on solid hydrophilic surfaces. *Sci. Adv.* **6**, eaax0746 (2020).
37. J. R. Panter, Y. Gizaw, H. Kusumaatmaja, Multifaceted design optimization for superomniphobic surfaces. *Sci. Adv.* **5**, eaav7328 (2019).

38. T. L. Liu, C.-J. C. Kim, Repellent surfaces. Turning a surface superrepellent even to completely wetting liquids. *Science* **346**, 1096–1100 (2014).
39. A. Tuteja *et al.*, Designing superoleophobic surfaces. *Science* **318**, 1618–1622 (2007).
40. D. Liao, M. He, H. Qiu, High-performance icephobic droplet rebound surface with nanoscale doubly reentrant structure. *Int. J. Heat Mass Transf.* **133**, 341–351 (2019).
41. X. Zhang *et al.*, Multibioinspired slippery surfaces with wettable bump arrays for droplets pumping. *Proc. Natl. Acad. Sci. U.S.A.* **116**, 20863–20868 (2019).
42. C. Chen, D. Weng, A. Mahmood, S. Chen, J. Wang, Separation mechanism and construction of surfaces with special wettability for oil/water separation. *ACS Appl. Mater. Interfaces* **11**, 11006–11027 (2019).
43. D. Monga *et al.*, Quasi-liquid surfaces for sustainable high-performance steam condensation. *ACS Appl. Mater. Interfaces* **14**, 13932–13941 (2022).
44. L. Zhang, Z. Guo, J. Sarma, X. Dai, Passive removal of highly wetting liquids and ice on quasi-liquid surfaces. *ACS Appl. Mater. Interfaces* **12**, 20084–20095 (2020).
45. L. Zhang, Z. Guo, J. Sarma, W. Zhao, X. Dai, Gradient quasi-liquid surface enabled self-propulsion of highly wetting liquids. *Adv. Funct. Mater.* **31**, 2008614 (2021).
46. H. Teisala, P. Baumli, S. A. L. Weber, D. Vollmer, H. J. Butt, Grafting silicone at room temperature–A transparent, scratch-resistant nonstick molecular coating. *Langmuir* **36**, 4416–4431 (2020).